

A Study on Gold-Silver Alloy Electrodeposition from Pyrophosphate-Cyanide Electrolyte Using Polyethylenimine-KSeCN Additives

Kubra Akben*, Servet Timur

Department of Metallurgical and Materials Engineering, Istanbul Technical University, 34469 Maslak, Istanbul, Turkey

*E-mail: hk.akben@gmail.com

Received: 27 October 2017 / Accepted: 3 January 2018 / Published: 6 March 2018

This paper presents the electrodeposition of gold-silver alloys from pyrophosphate–cyanide baths in the presence of a brightener couple, polyethylenimine (Mw=600 g/mol) and KSeCN. The nanocrystalline (X-ray diffraction) single phase electrodeposits with gold content ranging from 69 to 78 wt% (energy dispersive spectroscopy) are obtained galvanostatically. The influence of the polyethylenimine and KSeCN on the reduction kinetics of gold-silver alloy electrodeposition and on the mechanism of the electrodeposition process was studied by cyclic voltammetry and chronoamperometry. We observe that polyethylenimine polarizes the alloy deposition to high cathodic potentials and enhances the gold content from ca. 45 to 75 wt% in a current density range from 5 to 10 mA.cm⁻² with the support of KSeCN additive. Moreover, the alloy electrodeposition is found to proceed by a progressive nucleation and diffusion-controlled 3D growth mechanism with the addition of the brightener couple. We also discuss the morphological (scanning electron microscopy) and color changes in the presence of additives. Bright and coherent gold-silver alloy deposits are produced using the synergistic effects of polyethylenimine and KSeCN.

Keywords: Electrodeposition, Gold alloy, Silver, Brightener, Pyrophosphate–cyanide bath

1. INTRODUCTION

The superior physicochemical properties and appearance of gold make it a widely used metal in the jewelry, decorative and technological industries. However, economic considerations for gold usage have induced researchers to focus on reducing the amounts of gold used in these industries. For this reason, the electrodeposition of lower karat gold–silver alloy [1-3] and used industrially for decades through alkaline cyanide baths. Mostly, it can be used as an intermediate coating with a 23 - 24 karat gold finish providing high oxidation resistance. The intermediate layer is mostly applied in order to

prevent tarnish of thin gold deposits that is associated with diffusion of the base metal through the coating and porosity of the coating. Industrially, this layer is usually nickel, but some people are sensitive to nickel and can develop a form of dermatitis. Due to these reasons, the use of nickel is not preferred in trappings, and is strictly restricted by EU legislation.

Gold electroplating baths are mostly based on cyanide salts. However, owing to the strong toxicity of cyanide and environmental concerns, investigations have leaned toward non-cyanide based electrolytes [4-6], although the stability of these electrolytes is relatively low. As a result, the coherency and brightness of deposits are poor [7]. Hence, the industrial practice of these baths is considerably restricted. Considering this fact, focusing on buffer salts based electrolytes with no free cyanide addition [8], such as pyrophosphate-cyanide baths [9, 10], can offer a reasonable solution. In these baths, cyanide is only used as a stable complex form of gold or silver.

The voltammetric behavior and interfacial chemistry of gold-silver alloy electrodeposition from high cyanide baths have been investigated in detail [11-13]. However, the codeposition of gold and silver from pyrophosphate buffered baths containing no free cyanide has not yet been investigated. Here, it should also be stated that various bath compositions and operating conditions have been reported in the patent literature [14, 15], and the scientific literature is mostly restricted to the patents. A comprehensive investigation into the electrokinetic behavior of pyrophosphate gold-silver baths, which are effective on coating properties, is still lacking.

In modern electroplating, it is well understood that adequate brightness is provided by the use of organic and inorganic substances in small amounts [1, 16], although gold codeposition with other metals improves brightness. The most important effects of additives are generally classified into two groups, as leveling and brightening [16-18], but it is complicated to define the definitive role of an additive in this manner. However, it can be the basic and straightforward way to define the roles of additives as single or multiple groups of (a) grain refinement of the deposit, (b) polarization, (c) depolarization of the cathode which is also observed as catalyzing of the deposition and enhancing the current values in the same potential interval, (d) the change of crystal orientation, (e) the incorporation of additive in the coating, and (f) widening of the current density range. In many cases, the use together of two or more additives, which are responsible for different roles, improves the deposition brightness and quality sufficiently. This phenomenon is expressed as the synergistic effect of additives in many studies [19, 20].

Polymeric additives have been used in many electrolytes in industry, such as zinc, copper, and nickel plating baths. However, the effects of only a few additives have been reported in papers. The commonly reported ones are polyethylene glycol (PEG) and polyacrylamide (PAM) [21-23]. Especially in recent researches, polyethylenimine (PEI) has been investigated in zinc electrolytes [24, 25]. Ren [26] studied the role of PEI in gold electrodeposition in a cyanide free electrolyte, and confirmed the inhibitory effect of PEI, which resulted in more negative nucleation overpotential. Additionally, PEI's remarkable adsorption and inhibition effect on silver electrodeposition was reported [27, 28]. Also, inorganic additives can be used for brightening with a different type of mechanism. Selenium is the most industrially used inorganic additive in silver-cyanide electrolyte. It was shown that the accumulation of selenium at electrode / electrolyte interface leads to enhancement

of the silver deposition rate, and this was termed the catalytic effect of selenium and observed as rising current transients in studies [29, 30].

In this paper, we investigated the synergistic effect of an organic, polyethylenimine (Mw 600) (PEI), and an inorganic, KSeCN (Se), additive on gold-silver alloy electrodeposition from pyrophosphate based electrolytes. The effects on surface morphology, electrochemical and electrocrystallization mechanisms were discussed.

2. EXPERIMENTAL

2.1 Plating Methods and Materials

Hull cell studies were conducted to determine the range of operating current density, which forms bright gold alloy coatings. Electrodeposition was carried out using a 267 ml standard cell at a constant current of 0.2 A, at a temperature of 60°C for 5 minutes, unless otherwise stated. The electrolyte was stirred using a magnetic stirrer at a speed of 350 rpm during all galvanostatic plating and Hull cell experiments. The degree of agitation of the bath also plays an important role in determining the brightness level. But in this paper the effect of agitation will not be discussed. Overall, stirring speed was kept constant in the experiments.

The Hull cell and galvanostatic plating experiments were carried out using two-electrode configuration consisting of the platinized titanium mesh electrode acting as the anode and nickel-plated copper electrode acting as the cathode in the electrolyte. 2x4 cm² cathodes were used in galvanostatic plating. The nickel-plated copper cathodes were firstly activated by cathodic treatment (conditions: 20 mA.cm⁻² for 1 min. at 50-55 °C) in 60 g L⁻¹ KCN and 60 g L⁻¹ KOH solution. After adequate rinsing with distilled water, the sample was immersed in 1M H₂SO₄ for 10 s and then the second rinsing was applied. The galvanostatic plating cell had a volume of 250 cm³. The temperature was 60°C for all platings. KSeCN and PEI (Mw=600 g/mol) were acquired from Sigma Aldrich and Alfa Aesar, respectively. Analytical grade chemicals and distilled water were used to prepare all the solutions. The bath compositions and operating conditions used in Hull cell experiments are presented in Table 1.

Table 1. The bath compositions and operating conditions used in Hull cell experiments.

Bath Composition (abbreviations in text)	Concentration (g L ⁻¹)	Operating Conditions
KAu(CN) ₂ (Au)	4	Anode: Ni coated copper Cathode: Platinized titanium mesh
KAg(CN) ₂ (Ag)	3	
Potassium Pyrophosphate- K ₄ O ₇ P ₂ (P)	80	Temperature: 60°C pH: 10 Cell current: 0.2 A
KSeCN (Se)	1-5 ppm	
Polyethylenimine, Mw=600 (PEI)	0.5-1-2.5	

2.2 Electroanalytical Characterization

A standard three-electrode cell in a volume of 50 cm³ was used in cyclic voltammetry and chronoamperometry. The working electrode (a plate having 0.09 (0.3x0.3) cm² surface area) and the

counter electrode were made of platinum. The reference electrode was standard calomel electrode (SCE), and all potential values were reported vs. SCE. The cyclic voltammetry experiments were performed at a sweep rate of 50 mV s^{-1} . In all voltammograms, the fifth cycle corresponding to steady voltammogram was represented. For chronoamperometric analysis, first, the potential was held at 0.0 V for 10 s then stepped up to working potential to initiate nucleation and growth on the electrode. All the electrochemical analyses were conducted by Gamry PCI4/750TM potentiostat.

2.3 Characterization

The morphology of the electrodeposits coated in the presence and absence of the additives was analyzed by field emission scanning electron microscope (FEG-SEM, Jeol JSM 7000F). The quantitative composition analysis was evaluated by energy dispersive spectroscopy (EDS). The measurement was replicated five times for each sample through the coating surface. Moreover, through the thickness, ten different points were analyzed for each sample.

Minolta CM-503i Spectrophotometer was used for color measurements. The results were recorded using the CIELab color measurement system. The jewelry industry requires a system to standardize color between manufacturers and uses CIELab coordinate system [31]. CIELab is an internationally recognized color measuring system that was developed by CIE (Commission Internationale de l'Eclairage) and expresses the color as three-dimensional coordinates: L^* , a^* , and b^* . These coordinates describe all colors visible to the human eye. L coordinates changes between black ("0") to white ("100"), showing lightness. The values of a^* and b^* show the color change between green (-) to red (+) and blue (-) to yellow (+), respectively. This system was used to describe the color of the surface of the electrodeposits and the measurements were also compared with the color measurements of standard jewelry alloys and published color results [31-33]. The color measurements were done for five different portions of each sample. The arithmetic mean values of five measurements are presented.

The structural characterization was investigated by X-ray diffraction (XRD), using a Philips PW-3710 with a $\text{CuK}\alpha$ radiation ($\lambda = 1.54056 \text{ \AA}$). The X-ray peak broadening analysis, Williamson-Hall (W-H), is used to provide a comparative evaluation of crystallite size depending on the brightener couple addition.

The Vickers microhardness test was performed under 10 g load using a ShimadzuTM microhardness tester. The result of the microhardness test was the arithmetic mean, and standard deviation of 15 successive indentations.

3. RESULTS AND DISCUSSION

3.1 Hull cell testing

Hull cell test is a simple method that allows evaluating the bright and matt current density ranges via a single experiment. This method was applied for the optimization of the concentration of

bath constituents and operating conditions to achieve bright gold-silver alloy coating in a wide current density range.

In Fig. 1, the effect of electrolyte content and the addition of PEI and Se additives on the bright current density range and cathode color is presented. This figure was designed from photographs of Hull cathodes and Hull cell ruler. As seen in fig. 1a, a matt gold coating that darkens with increasing current through the cathode is obtained with the only Au ($\text{KAu}(\text{CN})_2$) added P ($\text{K}_4\text{O}_7\text{P}_2$) bath. The addition of Ag ($\text{KAg}(\text{CN})_2$) to this bath results in a semi-bright coating with a color trend of silver and green (see fig.1b). 0.5-1-2.5 g.L^{-1} PEI concentrations were studied. The best gloss result is 2.5 g.L^{-1} PEI. The result of concentration level study of Se among 1 and 5 ppm, and 5 ppm Se co-addition with PEI ensures a completely bright coating. As seen in Fig. 1c, with only 2.5 g.L^{-1} PEI addition to the electrolyte, although the brightness is increased, it is not sufficient. Finally, the co-addition of PEI and Se provides a completely bright coating between 0-10 mA.cm^{-2} current density (Fig. 1d). However, after about 5 mA.cm^{-2} , the color changes from metallic silver to greenish silver.

3.2 Galvanostatic Electrodeposition

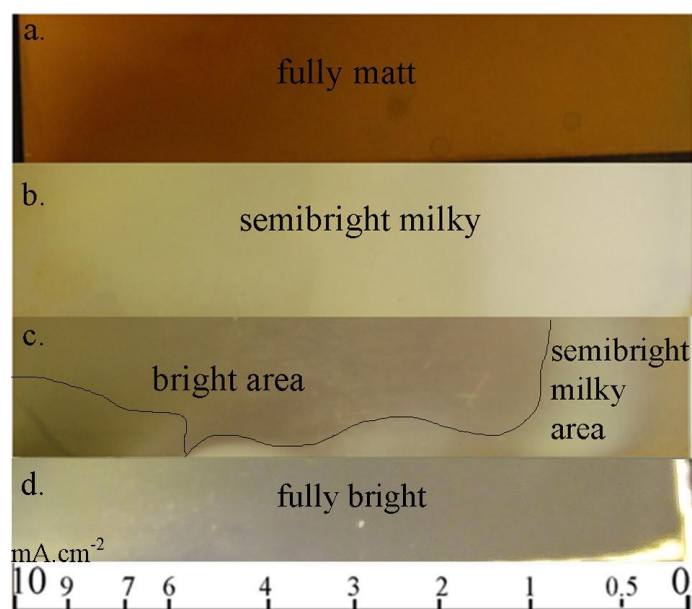


Figure 1. Hull cathodes obtained from a) 4 g.L^{-1} $\text{KAu}(\text{CN})_2$ + 80 g.L^{-1} $\text{K}_4\text{O}_7\text{P}_2$, b) 4 g.L^{-1} $\text{KAu}(\text{CN})_2$ + 80 g.L^{-1} $\text{K}_4\text{O}_7\text{P}_2$ + 3 g.L^{-1} $\text{KAg}(\text{CN})_2$, c) 4 g.L^{-1} $\text{KAu}(\text{CN})_2$ + 80 g.L^{-1} $\text{K}_4\text{O}_7\text{P}_2$ + 3 g.L^{-1} $\text{KAg}(\text{CN})_2$ + 2.5 g.L^{-1} PEI, d) 4 g.L^{-1} $\text{KAu}(\text{CN})_2$ + 80 g.L^{-1} $\text{K}_4\text{O}_7\text{P}_2$ + 3 g.L^{-1} $\text{KAg}(\text{CN})_2$ + 2.5 g.L^{-1} PEI + 5 ppm Se electrolytes.

The optimum current density range, which was determined by the Hull cell testing, was tested using galvanostatic electrodeposition. It should be highlighted here that, after a few electroplating operations in the same bath, it starts to plate in the same color. For this reason, the bath should be activated before use. For activation, step 5 mA.cm^{-2} is applied for 10 minutes to a cathode having 8 cm^2 surface.

The images of electrodeposits are shown in Fig. 2. When the coating is electrodeposited without any additive ($4 \text{ g L}^{-1} \text{ Au} + 3 \text{ g L}^{-1} \text{ Ag} + 80 \text{ g L}^{-1} \text{ pyrophosphate (P)}$), it has a semi-matte appearance and poor adhesion; see Fig. 2a. Only Se addition to the electrolyte induces nonuniform, semi-matte appearance. The addition of Se and PEI together makes the coating uniform and bright.

Fig. 2b demonstrates the color change of samples according to increased current density. As can be seen clearly, at more than 5 mA.cm^{-2} current density, color tends to change to green, though all samples are bright.

3.3 Deposit Morphology

SEM was employed to study the surface morphology of the deposits. Fig. 3 illustrates the morphological change depending on the additives, the current density, and the thickness. In the absence of the brightener couple, the deposit is rough and milky and grain sizes range from ca. 100 to 400 nm (see Fig. 3-1). With Se addition to the electrolyte, nonuniform morphology having smaller or larger grains is obtained (see Fig. 3-2).

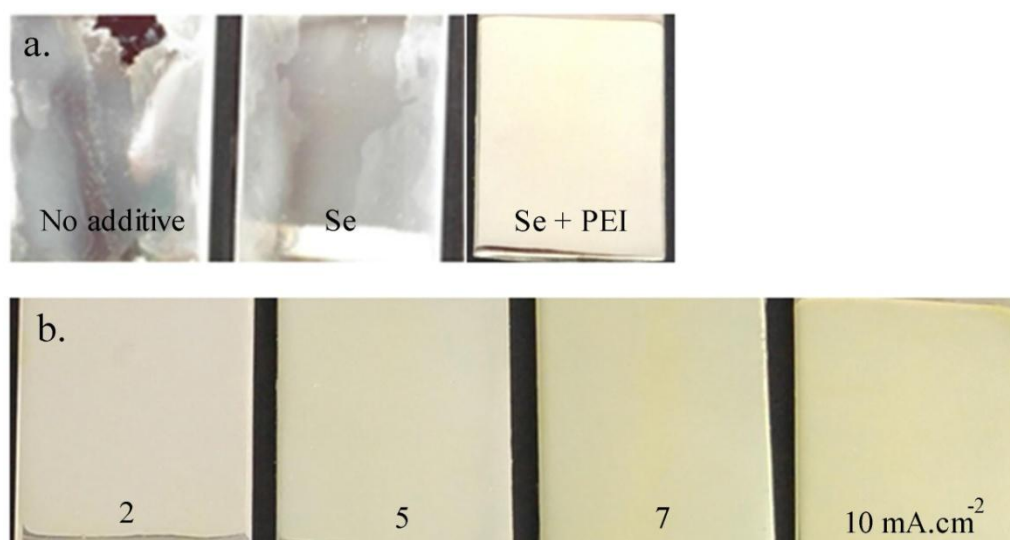


Figure 2. Photos of samples: a) showing the effect of Se and PEI addition to the electrolyte (at 5 mA.cm^{-2} for 5 min.), b) showing the effect of current density (2-5-7-10 mA.cm^{-2} for 5 min. with the optimum electrolyte composition in Table 1).

However, only PEI addition leads to smaller grains in the morphology as seen in Fig. 3-3. But, PEI addition is not sufficient for a fully bright deposit. More smooth and uniform morphology is obtained by the brightener couple addition, Se and PEI (Fig. 3-4), and the grain size decreases to ca. 20 to 80 nm. Moreover, the effect of the current density on the morphology of the coatings that were plated with brightener couple was investigated. It is obvious that the sample electrodeposited at a current density of 2 mA.cm^{-2} has larger grains in the smooth morphology than the sample coated at 5 mA.cm^{-2} , as shown in Figs. 3-5 and 3-4, respectively. The deposit coated at a current density of 7 and

10 mA.cm⁻² has small grains similar to those at 5 mA.cm⁻², but nodular growth is observed in the morphology of sample coated at 10 mA.cm⁻² (see Fig. 3-7). Despite the nodular growth, the coating has a bright appearance. The nodular growth is also observed in the case of even thicker coatings. Figs. 3-8 and 3-9 show the effect of thickness increase in deposits electrodeposited at a current density of 5 mA.cm⁻². The thickness of the coatings is 1.4, 2.9 and 4.0 μm for samples electrodeposited for 5, 10, and 20 min, respectively. We observe that the thickest coating has more nodular growth. It is also pointed out that while the appearance of 2.9 μm coating is bright, the 4.0 μm coated one has a slight hazy appearance, visually.

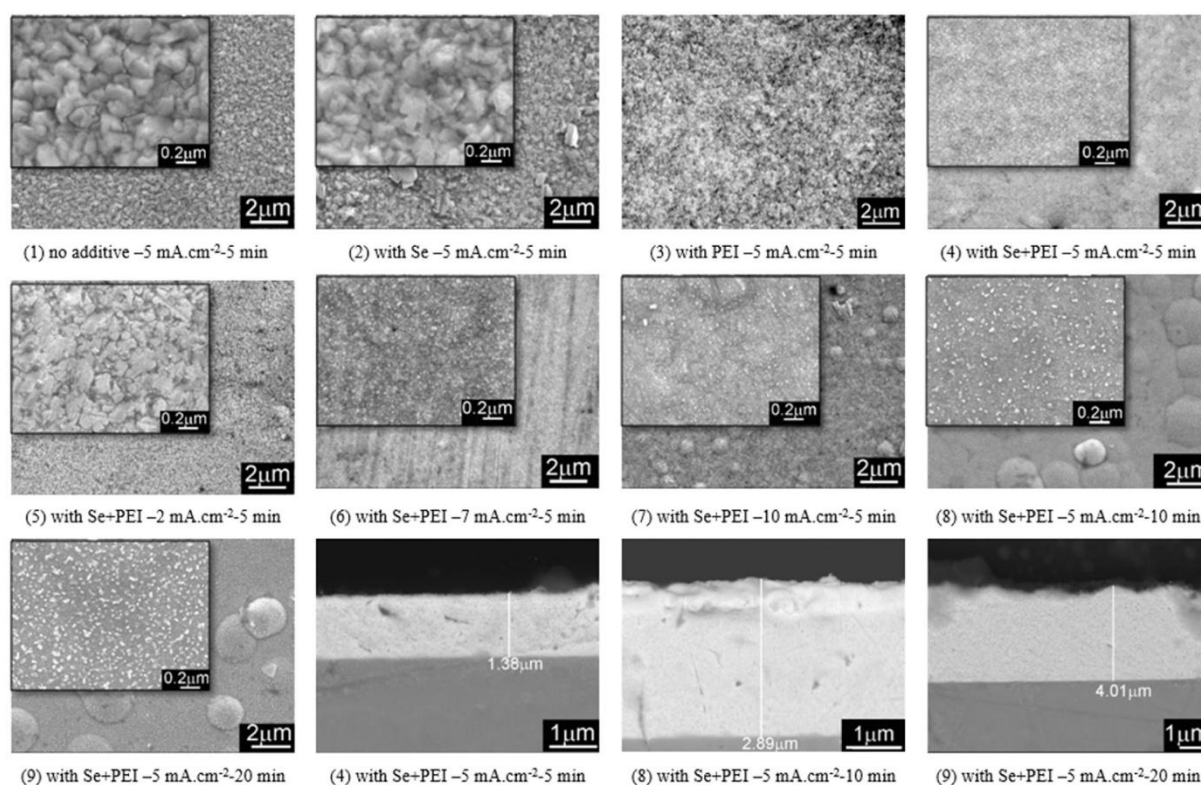


Figure 3. The morphological change depending on the additives, current density, and thickness.

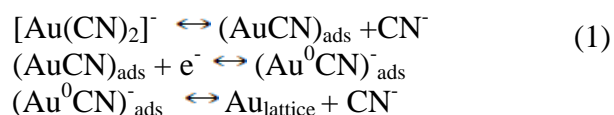
Efficiency was calculated for 5, 10, and 20 min. coated samples from Faraday's law of electrolysis. 5 and 10 min. coatings have similar efficiency, around 93 % and 96 %, respectively. Nevertheless, efficiency decreased to 67 % for the 20 min. coated one. We suspect that after 10 min. the process differs either due to accumulation of decomposition products in the bath, or surface coverage by different additives.

3.4 Cyclic Voltammetry

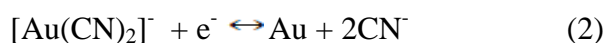
The effects of additives on the kinetics of electrochemical deposition were investigated with cyclic voltammetry technique and the reduction potential regions of gold and silver were identified. The solutions used in the electrochemical analysis are presented in Table 2. Higher gold content is

used in electrochemical analysis in order to observe the gold reduction peak easily. But in galvanostatic plating, decreasing the gold content in the bath formulation was intended to reduce the cost of the bath (see section 3.1 Hull cell testing). For this reason, different amounts of gold were used in electrochemical analysis and galvanostatic plating.

Fig. 4 shows the CV curves for gold reduction in two different electrolytes. In $\text{KAu}(\text{CN})_2$ (line S1), the CV curve shows two irreversible cathodic reduction peaks. At low cathodic potentials, the gold reduces from $\text{Au}(\text{I})$ cyanocomplex by chemical adsorption of a cyanide species, and this is followed by a charge transfer reaction, according to Eq. (1) [34, 35]



It was reported that at high cathodic potentials the direct reduction of $\text{Au}(\text{I})$ cyanocomplex to metallic gold occurs, according to the Eq. (2) [13, 36].



The gold reduction at low cathodic potentials is around -0.77 V (see Fig. 4- peak a). At high cathodic potentials gold reduction occurs by a Tafel type current density growth due to the hydrogen evolution reaction occurring simultaneously after ca. -1.1 V (peak b). In S2 curve, with the interaction between the pyrophosphate and gold cyanide species, the characteristic of reduction peak at high cathodic potentials changes and the cathodic peak is observed at -1.25 V (peak d).

Table 2. Electrolyte compositions used in electrochemical analysis.

Electrolyt e	$\text{KAu}(\text{CN})_2$ (g L^{-1})	$\text{KAg}(\text{CN})_2$ (g L^{-1})	$\text{K}_4\text{O}_7\text{P}_2$ (g L^{-1})	PEI (g L^{-1})	Se (ppm)
S1	10	-	-	-	-
S2	10	-	80	-	-
S3	-	3	-	-	-
S4	-	3	80	-	-
S5	10	3	80	-	-
S6	10	3	80	2.5	-
S7	10	3	80	-	5
S8	10	3	80	2.5	5

The CV curve in Fig. 5 shows the reduction behavior of $\text{KAg}(\text{CN})_2$. The peak observed at low cathodic potentials indicates the reduction of silver oxide species, which are formed in the previous anodic cycle. This aspect will not be discussed in this paper, because it would be beyond the aim of this paper. The reduction of $\text{KAg}(\text{CN})_2$ is observed at ca. -0.87 V (peak a) in S3 curve (without pyrophosphate). On the other hand, with the addition of pyrophosphate species to the electrolyte, the

reduction behavior of $\text{KAg}(\text{CN})_2$ changes and two reduction peaks occur at about -0.62 V (peak b) and -0.91 V (peak c).

Fig. 6 illustrates the deposition behavior when both the metal ions are in the pyrophosphate electrolyte with or without brighteners. In the literature, electrodeposition of gold-silver alloy was investigated from highly concentrated cyanide electrolytes and two cathodic maximums were recorded for simultaneous deposition of gold and silver [11, 12]. However, in the S5 curve in Fig. 6 (the electrolyte without brighteners) there are three cathodic maximums referred to as (peak a), (peak e) and (peak 3). The first cathodic maximum (peak a) at approximately -0.62 V is the silver reduction peak at low cathodic potentials. Increasing the cathodic voltage beyond -0.75 V, gold starts to be deposited simultaneously with silver. As the cathodic potential increases, the gold content increases in the deposit as well. The simultaneous electrodeposition of gold-silver could be identified with two cathodic maximums at ca. -0.87 V (peak e) and -1.25 V (peak 3) in the pyrophosphate-cyanide electrolyte. It is less explicit to assign reduction mechanisms to the voltammogram in the alloy system. On the other hand, it can be supposed that the chemical-electrochemical reduction mechanism displayed in Eq. (1) can take place at low cathodic potential for both metals simultaneously. Similarly, at high cathodic potential the reduction occurs via direct electrochemical reduction mechanism defined in Eq. (2) for simultaneous metal deposition.

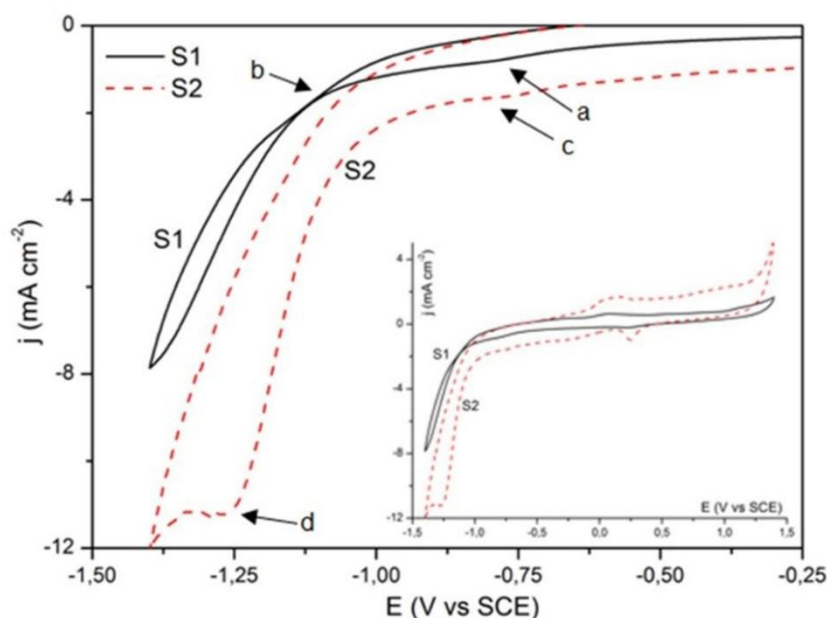


Figure 4. CV curves registered in: (S1) $\text{KAu}(\text{CN})_2$, (S2) $\text{KAu}(\text{CN})_2$ + pyrophosphate.

When PEI is added to the Au-Ag electrolyte as a brightener, only two cathodic maximums are observed in the negative going scan as shown in Fig. 6-S6 curve. It can be noticed that PEI has a considerable retarding effect on simultaneous deposition of gold and silver. The first cathodic peak (c) in S6 curve is the polarized silver electrodeposition at low cathodic potentials. Moreover, the main polarization effect is revealed with the disappearance of the second cathodic peak (peak e) observed in S5 curve (without brightener). With the addition of PEI, this peak is polarized beyond the -1.0 V that

merges with the third cathodic peak observed in S5 curve (without brightener). This broad cathodic peak has two shoulders at ca. -1.0 and -1.25 V.

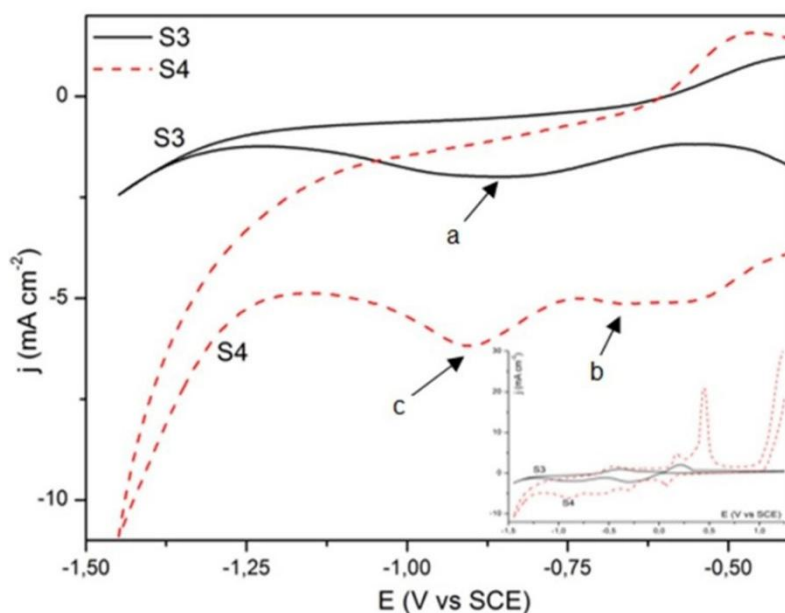


Figure 5. CV curves registered in: (S3) $\text{KAg}(\text{CN})_2$, (S4) $\text{KAg}(\text{CN})_2$ + pyrophosphate.

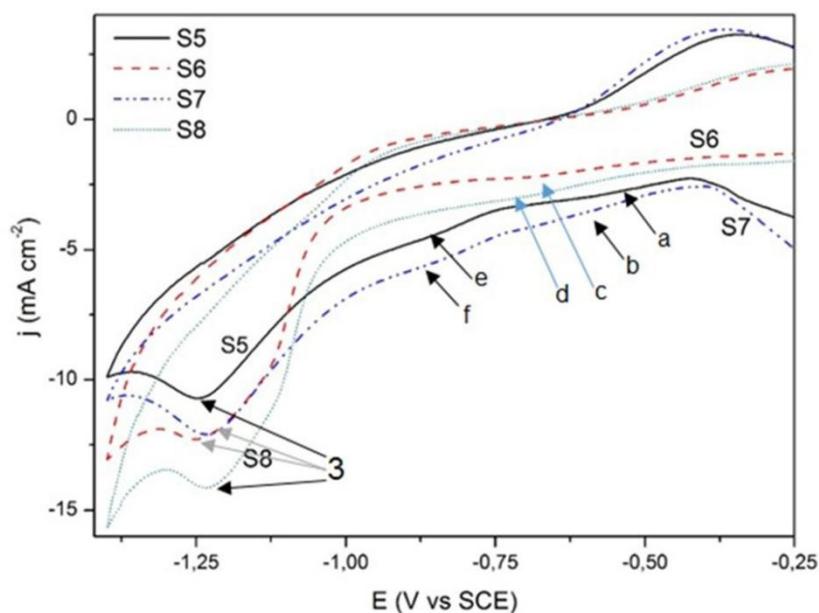


Figure 6. CV curves registered in: (S5) $\text{KAu}(\text{CN})_2$ + $\text{KAg}(\text{CN})_2$ + pyrophosphate, (S6) $\text{KAu}(\text{CN})_2$ + $\text{KAg}(\text{CN})_2$ + pyrophosphate +PEI, (S7) $\text{KAu}(\text{CN})_2$ + $\text{KAg}(\text{CN})_2$ + pyrophosphate +Se, (S8) $\text{KAu}(\text{CN})_2$ + $\text{KAg}(\text{CN})_2$ + pyrophosphate +PEI+Se.

The polarization effect is due to the adsorption of the PEI onto the electrode surface, which partially blocks the active electrode surface area. Therefore, the second cathodic peak (peak e) appears at more negative values, while the additive desorbs from the electrode surface. Applying more

negative potential than -1.0 V in PEI added electrolyte induces gold content increase in the deposit steeply. Apparently, by the retarding effect of PEI on gold and silver electrodeposition at low cathodic potentials, gold codeposition is enhanced at high cathodic potentials compared with silver. The suppressing effect of PEI on silver electrodeposition kinetic was indicated previously [27]. As mentioned in composition analysis section (EDS analysis shown in Table 3), the addition of PEI to the electrolyte induces the enhancement of gold content approximately from 50 wt% to 75 wt%.

The addition of Se to the electrolyte modifies the reduction process in a different manner. The current density values of cathodic peaks (see line S5 - peaks: a, e, 3) increase with the addition of Se seen in Fig 6 - S7 curve (peaks: b, f and 3). The increase of current density at the same potential interval can be attributed to the catalytic effect of Se, which causes the increase in the rate of gold and silver reduction. The catalytic effect of widely known brightener Se is a well-reported phenomenon [29, 30], that the accumulation of it on the surface enhances the deposition rate of silver. We observe this effect of Se on gold-silver deposition with CV experiments.

Fig 6 – curve S8 presents the effects of adding the combination of the brightener couple, PEI and Se. When a combination of brighteners is added to the electrolyte, two similarly polarized cathodic peaks are observed as in the S6 curve (only with PEI addition), but also with the Se addition, the peak currents increase similarly as seen in S7 curve (only with Se addition). This means that the individually observed effects of brighteners are combined when the brightener couple is added to the electrolyte. While PEI has a polarization effect which is retarding simultaneous deposition of the gold and silver, the current density values are increased with the addition of Se at the same potential interval.

3.5 Chronoamperometry

The chronoamperometric method has been utilized to study the nucleation and growth mechanism of electrodeposited gold-silver alloy with and without brightener couple (PEI and Se). Typical potentiostatic transient shows two negative potential regions between -0.78 to -0.87 V and -1.08 to -1.20 V (see Fig. 7) for two voltammetric peaks of gold-silver codeposition depicted in Fig. 6 (see line S5 - peaks: e, 3 (without brighteners)). Moreover, Fig. 8 shows the chronoamperometric curves only between -1.08 and -1.20 V for gold-silver codeposition with brightener couple. As mentioned previously, the reasons for this gold-silver codeposition with the brightener couple are polarized and recorded after cathodic potential -1.0 V.

As seen in Fig. 7a, at low cathodic potentials a double layer formation occurs in the first few seconds, which is observed as a sharp increase in current density profile; on the other hand, at high cathodic potentials, double layer charging is not observed. After that, typically the current rises up to a current maximum and it is followed by a decay; see Fig. 7 and 8. Then, the current converges to the limiting current density.

Considering the chronoamperometric results, the transients are fitted to the three-dimensional (3D) classical nucleation and diffusional growth model of Scharifker and Hills [37]. The model is described for two different nucleation processes. “Instantaneous” nucleation is defined as nucleation

occurring in all active sites at the beginning when potential is applied. In addition to this, “progressive” nucleation means that sites become active for nucleation during electrodeposition. However, these definitions are likely to cause confusion, because when the potential is applied, nuclei never form at once; they always form progressively [38]. In this respect, the instantaneous and the progressive nucleation mechanisms are referred to as fast and slow nucleation, respectively [38].

In Figs. 9 and 10, non-dimensional plots of I^2/I_m^2 vs. t/t_m are constituted from the experimental j - t transients in Figs. 7 and 8. I_m and t_m correspond to the maximum of the peak. Besides, the theoretical curves in Figs. 9 and 10 are calculated from the equations derived by Scharifker et al. [37] for progressive and instantaneous nucleation (Eq. (3) and (4), respectively).

$$\frac{I^2}{I_m^2} = \frac{1.2254}{\frac{t}{t_m}} \left\{ 1 - \exp \left(-2.3367 \left(\frac{t}{t_m} \right)^2 \right) \right\}^2 \quad (3)$$

$$\frac{I^2}{I_m^2} = \frac{1.9542}{\frac{t}{t_m}} \left\{ 1 - \exp \left(-1.2564 \left(\frac{t}{t_m} \right) \right) \right\}^2 \quad (4)$$

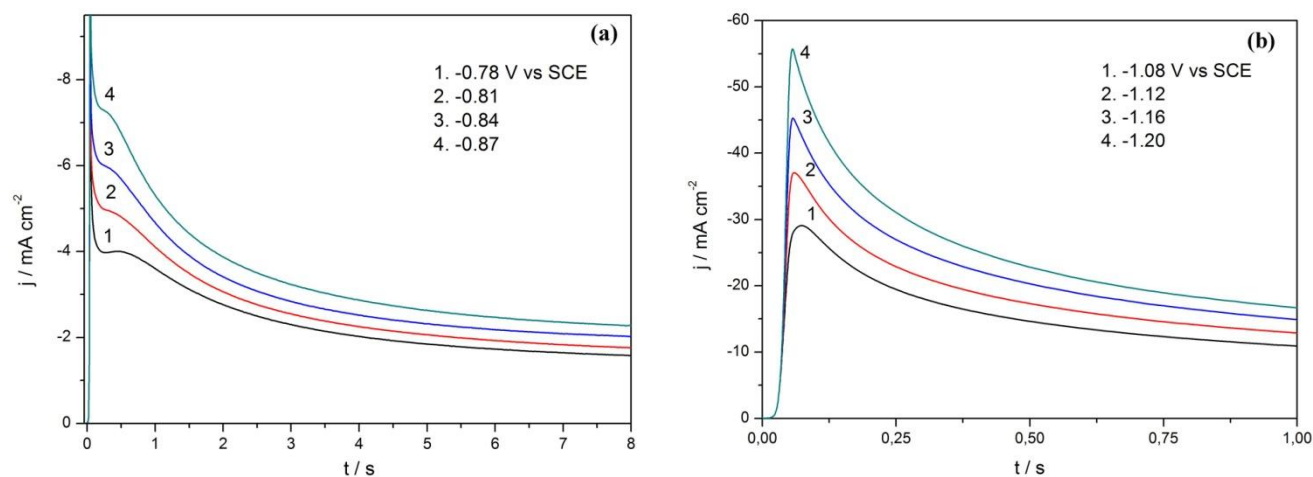


Figure 7. Potentiostatic j - t transients for gold-silver reduction in the absence of brighteners in solution (5) (a) from -0.78 to -0.87 V, (b) from -1.08 to -1.20 V.

It is found that the gold-silver alloy electrodeposition at lower overpotentials without brighteners follows a 3D instantaneous nucleation and growth mechanism. However, at high cathodic potentials, the nucleation mechanism is 3D progressive. In the presence of brightener couple, codeposition is polarized to high overpotentials and follows a 3D progressive nucleation and growth mechanism, as seen in Fig. 10. Nevertheless, the decaying portion of current is not completely fitted to the progressive side. This may be conceived as an additional process occurring besides the 3D diffusion controlled nucleation. However, it should also be noted that according to the form of the growth center (right circular cones, hemispheroids or paraboloids), the decaying portion of j - t transient can change, but the rising part of the transient is independent of the geometry of the growth center [38]. Figures 9 and 10 have proper fits in the rising part of the current up to the current maximum.

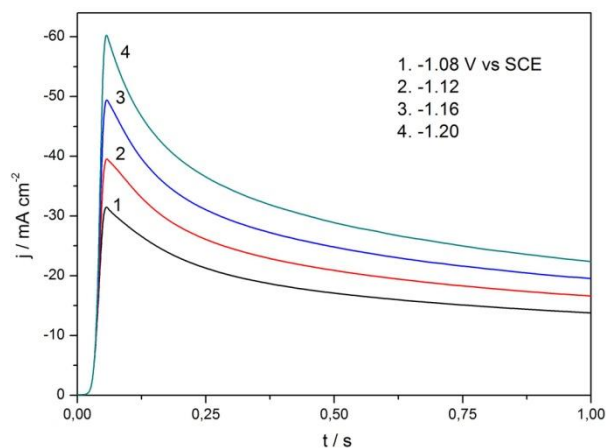


Figure 8. Potentiostatic j - t transients for gold-silver reduction in the presence of brighteners in solution (8), from -1.08 to -1.20 V.

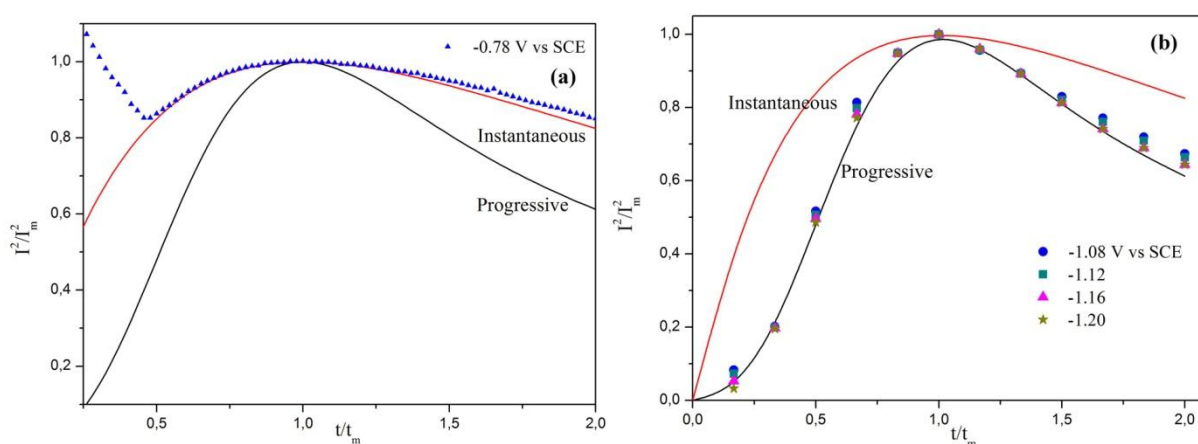


Figure 9. I^2/I_m^2 vs. t/t_m curves for deposition in solution (5), (a) -0.78 V, (b) from -1.08 to -1.20 V. The continuous lines correspond to the theoretically instantaneous (upper curve) and progressive (lower curve) nucleation and growth mechanism.

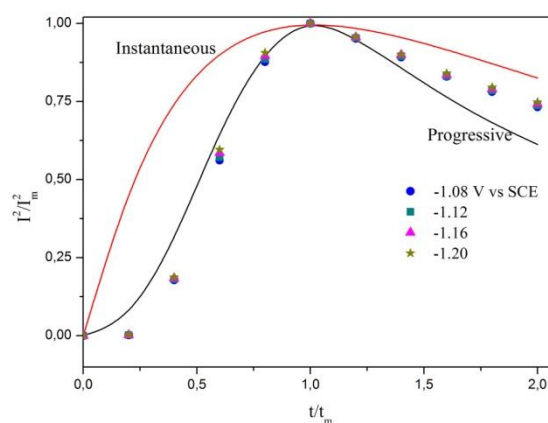


Figure 10. I^2/I_m^2 vs. t/t_m curves for deposition in solution (8), from -1.08 to -1.20 V. The continuous lines correspond to theoretically instantaneous (upper curve) and progressive (lower curve) nucleation and growth mechanism.

3.6 X-Ray Diffraction Analysis

The XRD patterns of electrodeposits are shown in Fig. 11. Single-phase gold-silver face centered cubic (FCC) layers are grown at all samples. Some of the samples have copper diffraction from the substrate. All deposits are found to have a slight (111) texture, as expected. The evaluation of the crystallite size is of great importance for the understanding of the effect of brighteners on reducing the crystallite size. Williamson-Hall (W-H) X-ray peak broadening analysis is used to provide a comparative evaluation of crystallite size depending on the brightener couple addition. This method examines two factors contributing to the peak broadening, lattice strain and grain size [39], and these factors are obtained considering full width at half maximum (FWHM) of peaks as a function of 2θ shown in Eq. (5), where β_{hkl} is the sum of the peak width, θ is the Bragg angle, k is the Scherrer constant, D is the crystallite size, ε is the strain and λ is the wavelength of the X-ray incident radiation.

$$\beta_{hkl} \cos \theta = \left(\frac{k\lambda}{D} \right) + (4\varepsilon \sin \theta) \quad (5)$$

Firstly, $\beta_{hkl} \cos \theta$ (on the y axis) is plotted against $4 \sin \theta$ (on the x axis). Next, a linear fit is applied to this plot. The crystallite size is estimated from the y-intercept of the linear fit, whereas the strain ε is estimated from the slope. Providing that the slope of the fit (strain) is zero, the broadening is occurring due to the decrease in crystallite size only. As seen in Table 3, while the crystallite size of deposit is about 89 nm with no brightener addition (sample 1), the crystallite size decreases approximately to 44 nm with the addition of the brightener couple (sample 3). In addition, while applied current density is increased from 2 to 5 mA.cm⁻² (samples 3 and 4, respectively), the crystallite size decreases, too. Increase in current density beyond 5 mA.cm⁻² does not result in any distinct change of the crystallite size.

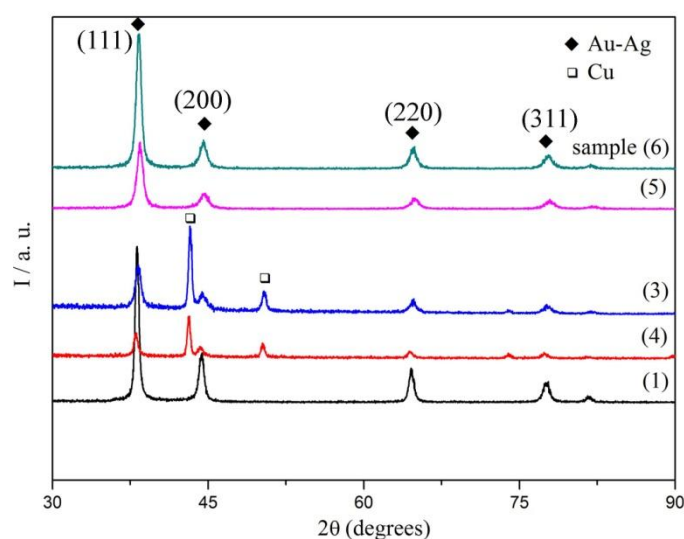


Figure 11. XRD patterns of electrodeposited samples (1) without brightener at 5 mA.cm⁻², (4) with brighteners at 2 mA.cm⁻², (3) with brighteners at 5 mA.cm⁻², (5) with brighteners at 7 mA.cm⁻², (6) with brighteners at 10 mA.cm⁻².

3.7 Color Measurement

The L^* , a^* , b^* color values of electrodeposits and reference samples (pure gold, silver and 3N, 4N reference samples) were measured and presented in Table 3. The color values of pure gold and silver and 3N, 4N standard samples (which have 75 wt% gold) are consistent with measurements in literature [31-33]. The samples 1 and 2 (without brightener and with only Se, respectively) are not bright and have a whitish appearance. The samples 3, 4, 5, 6 and 7 plated with the brightener couple (Se+PEI) have a bright appearance. The color of these samples is compared with the color of references in Fig. 12. Increasing current density from 2 to beyond 5 mA.cm⁻² (samples 4 and 3) results in a color change going through green and yellow sides. Samples 3, 5 and 6 (coated at 5, 7 and 10 mA.cm⁻²) have nearly the same color values and they are in the same region of Fig. 12. However, pure gold and silver and 3N, 4N standard gold alloys are in different regions of the figure according to the electrodeposits. Only the b components of 3N and 4N standard alloys are close to electrodeposited samples (coated at 5, 7 and 10 mA.cm⁻²). The a^* components of these electrodeposited samples are greener than standard samples. Clearly, 2 mA.cm⁻² coated sample is near the pure silver, but it has a slightly greener hue.

Additionally, sample 7 and 8 electrodeposited for 10 and 20 min have nearly the same color values as 5 min. coated samples (coated at 5, 7 and 10 mA.cm⁻²) as seen in Table 3. These color values presented in Table 3 should be used for controlling color of electrodeposited samples.

3.8 Composition Analysis

Table 3. L^* , a^* , b^* color values and composition % and average crystallite sizes.

No	Coating conditions	L	a	b	wt% gold	Average crystallite size (nm)
1	5 mA.cm ⁻² , 5 min., electrolyte (Au + Ag + P) with no additive	96.7	-3.2	14.5	45±1	89.1
2	5 mA.cm ⁻² , 5 min., electrolyte (Au + Ag + P) with Se	97.3	-3.3	13.1	50±2	56.7
3	5 mA.cm ⁻² , 5 min., electrolyte* with Se and PEI	93.6	-7.1	22.2	72±3	44.4
4	2 mA.cm ⁻² , 5 min., electrolyte*	100.3	-1.9	5.0	26±1	62.0
5	7 mA.cm ⁻² , 5 min., electrolyte*	91.6	-7.8	23.3	74±1	46.0
6	10 mA.cm ⁻² , 5 min., electrolyte*	91.6	-7.7	23.0	75±3	42.1
7	5 mA.cm ⁻² , 10 min., electrolyte*	90.3	-8.5	22.4	74±2	39.6
8	5 mA.cm ⁻² , 20 min., electrolyte*	89.8	-8.0	23.1	75±3	39.8
9	Standard 3N** gold alloy	80.2	3.8	24.4	75	
10	Standard 4N** gold alloy	79.3	5.8	21.1	75	
11	Pure gold	86.0	4.8	36.7	99.9	
12	Pure silver	98.8	-0.7	5.3	0	

*Optimum electrolyte composition mentioned in table 1.

** Standards common to Germany, France and Switzerland.

The compositions of coatings are presented in Table 3. The current density–composition relationship is shown in Fig. 13. The sample 4 electrodeposited at $2 \text{ mA}\cdot\text{cm}^{-2}$ has a considerably low gold content (ca. 26 wt%). With further increase of current density beyond $5 \text{ mA}\cdot\text{cm}^{-2}$, gold content of coating exceeds approximately 70 wt%. Electrodeposition at a current density of 7 and $10 \text{ mA}\cdot\text{cm}^{-2}$ results in a nearly same composition (ca. 75 wt %). The color values are related to the composition results. The increase of gold content to ca. 75 wt% with the increase in current density to $5\text{-}10 \text{ mA}\cdot\text{cm}^{-2}$ exhibits a color trend going through greener and yellower tone.

It is also pointed out that with addition of only Se to the electrolyte, gold content increases to ca. 50 wt% from 45 wt%, whereas the addition of both PEI and Se results in an increase of gold content to ca. 75 wt% for $5 \text{ mA}\cdot\text{cm}^{-2}$. The increase of coating thickness while keeping the current density constant at $5 \text{ mA}\cdot\text{cm}^{-2}$ does not induce the variation of composition significantly. The compositions throughout the cross sections of samples are between 69–78 wt% gold, 22–31 wt% silver up to $4.0 \mu\text{m}$.

3.9 Microhardness Measurement

In this study, the microhardness measurement is applied to the sample deposited for 10 min. at $5 \text{ mA}\cdot\text{cm}^{-2}$ which has $2.9 \mu\text{m}$ thickness and $74 \pm 2 \text{ wt} \%$ gold content. The mean microhardness value of the sample with standard deviation is $279 \pm 7.5 \text{ HV}$. In the literature, the Vickers hardness values were reported to be between 270–290 HV for gold-silver alloy (75 wt % gold) electrodeposits [40] and 130 HV for pure gold electrodeposit [41]. As can be seen, the microhardness result of this study is compatible with the literature, and gold-silver alloy coatings have higher microhardness values than pure gold deposit.

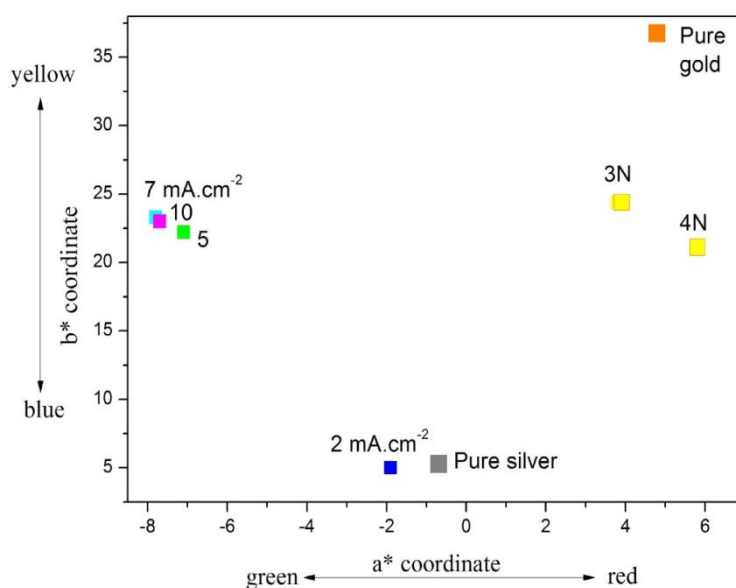


Figure 12. CIELab a^* , b^* coordinates of electrodeposits and reference samples.

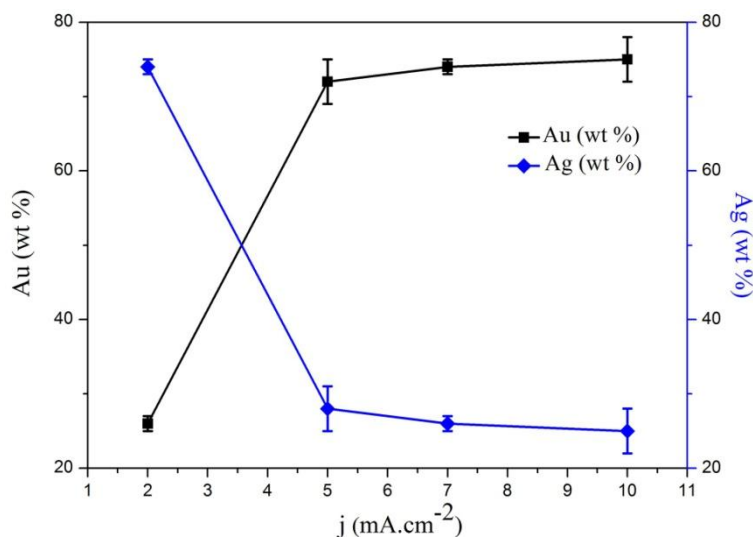


Figure 13. Composition (EDS) of samples as a function of c. d.

4. CONCLUSION

The findings of the present study demonstrate that PEI and Se are an effective brightener couple for Au-Ag alloy electrodeposition. While PEI polarizes the codeposition, Se catalyzes the deposition by increasing the current density values in the same potential interval. Cyclic voltammetry illustrates explicitly the polarization effect. The codeposition occurs at high cathodic potentials with a clear increase of the current density values with the addition of PEI and Se together. Moreover, EDS results reveal that the polarized codeposition induces gold content to increase up to approximately wt% 75, whereas without brighteners or only with Se addition gold content was ca. wt% 45-50. It means that PEI addition enhances gold content in alloy deposit. Based on chronoamperometric results, 3D instantaneous nucleation and growth at low cathodic potentials is polarized to high cathodic side with the addition of brighteners, and progresses as 3D progressive nucleation mechanism. It can be interpreted that the fast nucleation at low cathodic potentials polarizes to high cathodic side, and also that nucleation slows with the addition of brighteners. The surface morphology analysis of deposits indicates the combined effect of additives on refining the grain size and smoothening the deposit surface. The grain size is slightly smaller than 80 nm beyond 5 mA.cm⁻² in the presence of brighteners.

To sum up, this electrolytic bath can be used in the current density range of 2 - 10 mA.cm⁻². The gold content is 26 wt% for sample electrodeposited at a current density of 2 mA.cm⁻², and beyond 5 mA.cm⁻² the gold content is about 75 wt%. The color values are related to the composition results, and between 5 and 10 mA.cm⁻² are nearly the same, indicating that the coatings have nearly the same composition, around 75 wt%. By more than 2.9 microns thickness, a hazy appearance can be obtained. The composition throughout the cross sections of samples is between 69-78 wt % gold up to 4 μ m.

Consequently, in order to diminish the cost of a thick gold deposit, it can be a good alternative to use this smooth deposit as an intermediate coating with a thin, flash gold finish in the desired color, purity and low porosity, and thus conferring good corrosion resistance.

ACKNOWLEDGEMENTS

The authors would like to thank TUBITAK (The Scientific and Technological Research Council of Turkey) with project 112M044 and ITU (Istanbul Technical University) for BAP project 37419 for the financial support. Also, K. Akben is grateful to the TUBITAK for Ph.D. scholarship funding.

References

1. G. Bacquias, *Gold. Bull.*, 15 (1982) 124.
2. D.R. Mason, *Gold. Bull.*, 7 (1974) 104.
3. F.D. Gardner, R.E. Cornell, US Patent 3092559, (1963).
4. J. Chen, Y. Fang, Q. Qiu, L. You, J. Song, G. Zhang, G. Chen, J. Sun, *Green Chem.*, 13 (2011) 2339.
5. M. Saitou, T. Ota, A. Nakano, S.M. Asadul Hossain, *Surf. Coat. Technol.*, 201 (2007) 6947.
6. G. Baltrūnas, A. Valiūnienė, J. Vienožinskis, E. Gaidamauskas, T. Jankauskas, Ž. Margarian, *J. Appl. Electrochem.*, 38 (2008) 1519.
7. E.C. Estrine, S. Riemer, V. Venkatasamy, B.J.H. Stadler and I. Tabakovic, *J. Electrochem. Soc.*, 161 (2014) 687.
8. A. Dolati, M. Ghorbani, M.R. Ahmadi, *J. Electroanal. Chem.*, 577 (2005) 1.
9. A. Hrussanova, I. Krastev, *J. Appl. Electrochem.*, 39 (2009) 989.
10. S. Nineva, T. Dobrovolska, I. Krastev, *J. Appl. Electrochem.*, 41 (2011) 1397.
11. K. Márquez, R. Ortiz, J.W. Schultze, O.P. Márquez, J. Márquez, G. Staikov, *Electrochim. Acta.*, 48 (2003) 711.
12. B. Bozzini, G.P. De Gaudenzi, C. Mele, *J. Electroanal. Chem.*, 563 (2004) 133.
13. B. Bozzini, G.P. De Gaudenzi, C. Mele, *J. Electroanal. Chem.*, 570 (2004) 29.
14. W.L. Moriarty, A. Fletcher, US Patent 4121982, (1978).
15. J.M. Deuber, P. Stevens, US Patent 4088549, (1978).
16. L. Oniciu, L. Mureşan, *J. Appl. Electrochem.* 21 (1991) 565.
17. M Nunez, Metal electrodeposition, Nova Science Publishers Inc, (2005) New York, USA.
18. N. Kanani, Electroplating: Basic Principles, Processes and Practice, Elsevier Advanced Technology, (2004) Oxford, England.
19. K.O. Nayana, T.V. Venkatesha, *J. Ind. Eng. Chem.*, 26 (2015) 107.
20. M. Li, S. Luo, Y. Qian, W. Zhang, L. Jiang, J. Shen, *J. Electrochem. Soc.*, 154 (2007) 567.
21. N. Soruor, W. Zhang, E. Ghali, G. Houlachi, *Hydrometallurgy*, 171 (2017) 320.
22. J.P. Healy, D. Pletcher, M. Goodenough, *J. Electroanal. Chem.*, 338 (1992) 155.
23. S.J. Song, S.R. Choi, J.G. Kim, H.G. Kim, *Int. J. Electrochem. Sci.*, 11 (2016) 10067.
24. A.B. Hashemi, G. Kasiri, F.L. Mantia, *Electrochim. Acta.*, 258 (2017) 703.
25. S. J. Banik, R. Akolkar, *Electrochim. Acta.*, 179 (2015) 475.
26. X. Ren, Y. Song, A. Liu, J. Zhang, P. Yang, J. Zhang, G. Yuan, M. An, H. Osgood, G. Wu, *RSC Adv.*, 5 (2015) 64806.
27. Z. B. Lin, B. G. Xie, J. S. Chen, J. J., Sun, G. N. Chen., *J. Electroanal. Chem.*, 633 (2009) 207
28. S. Masaki, H. Inoue, H. Honma, *Met. Finish*, 96 (1998) 16.
29. T.P. Moffat, B. Baker, D. Wheeler, J.E. Bonevich, M. Edelstein, D.R. Kelly, L. Gan, G.R. Stafford, P.J. Chen, W.F. Egelhoff, D. Josell, *J. Electrochem. Soc.*, 149 (2002) C423.

30. B.C. Baker, C. Witt, D. Wheeler, D. Josell, T.P. Moffat, *Electrochem. Solid. St.* 6 (2003) 67.
31. C. Cretu, E. Van der Lingen, *Gold. Bull.*, 32 (1999) 115.
32. F.C. Levey, M.B. Cortie, L.A. Cornish, *Scripta Mater.*, 47 (2002) 95.
33. U. E. Klotz, *Gold. Bull.*, 43 (2010) 4.
34. Y.G. Li, W. Chrzanowski, A. Lasia, *J. Appl. Electrochem.*, 26 (1996) 843.
35. G. Holmbom, B.E. Jacobson, *J. Electrochem. Soc.*, 135 (1988) 787.
36. P. Bindra, D. Light, P. Freudenthal, D. Smith, *J. Electrochem. Soc.*, 136 (1989) 3616.
37. B. Scharifker, G. Hills, *Electrochim. Acta.*, 28 (1983) 879.
38. D. Pletcher, Z.Q. Tian, D.E. Williams, *Developments in electrochemistry*, Times by Aptara Inc, (2014) New Delhi, India.
39. Z. Zhang, F. Zhou, E. J. Laverna, *Metall. Mater. Trans. A.*, 34 (2003) 1349.
40. W. A. Fairweather, *Gold Bull.*, 10 (1977) 15.
41. M. Hosseini, S. Ebrahimi, *J. Electroanal. Chem.*, 645 (2010) 109.

© 2018 The Authors. Published by ESG (www.electrochemsci.org). This article is an open access article distributed under the terms and conditions of the Creative Commons Attribution license (<http://creativecommons.org/licenses/by/4.0/>).